Measurement 46 (2013) 3654–3661

Contents lists available at SciVerse ScienceDirect

Measurement

journal homepage: www.elsevier.com/locate/measurement

# Measurement and modeling of Bidirectional Reflectance Distribution Function (BRDF) on material surface

Hongyuan Wang *, Wei Zhang, Aotuo Dong

*Research Center for Space Optical Engineering, Harbin Institute of Technology, Harbin 150001, China*

ARTICLE INFO

*Article history:*
Received 25 May 2012
Received in revised form 21 March 2013
Accepted 11 July 2013
Available online 20 July 2013

*Keywords:*
Optical properties of surfaces
Bidirectional Reflectance Distribution Function (BRDF)
Measurement
Modeling
Error analysis

ABSTRACT

Measurement and modeling of Bidirectional Reflectance Distribution Function (BRDF) is made to describe optical scattering characteristics of the material surface. A measurement device of BRDF with the ability to real-time measurement is developed by the micro fiber spectrometer and three-dimensional turntables. The measured spectral range is from visible to near infrared with 2.4 nm wavelength resolution. The measured angular range is 0–360° in azimuth angle and 0–85° in zenith angle with 0.01° angle resolution. BRDF measurement on tinfoil and ceramic tile is made and the measurement error is no more than 6.05%. A six-parameter model of BRDF is built according to material surface characteristics. Based on the simulated annealing algorithm, the model parameters of BRDF are obtained through fitting processing of measured data and the maximal fitting error is 9.94%. The results show that the measuring accuracy of BRDF depends on the precision of measuring platform, the sensitivity of measuring instrument and the stability of illuminating light source, and the modeling accuracy of BRDF is closely related to the measured data and optimization modeling method. The measurement and modeling of BRDF may benefit future optical remote sensing, computer graphics and environmental surveillance.


## 1. Introduction

With the development of computer technology, the Bidirectional Reflectance Distribution Function (BRDF), as a theoretical concept that describes the directional reflection characteristics by relating the incident irradiance from a given direction to its contribution to the reflected radiance in another specific direction, is widely used in computer graphics [1,2], optical remote sensing [3,4], environmental monitoring [5,6], modeling of object characteristics [7] and other fields of scientific research [8,9]. For instance, BRDF can be used to study reflection characteristics of the material surface [10,11], which provides an important facility for object detection and recognition [12,13]. BRDF is usually obtained by experimental measurement. Generally, a spectral radiometer or digital camera is used to capture reflected information. Such equipment is usually much larger and heavier, which limits the measuring angle range to a great extent [14,15]. The measured zenith angle is 0–65° for most of the measurement equipments and it is necessary to improve measurement platform so as to extend the measuring angle and acquire more optical reflection information of the material surface for different lighting or viewing direction. At the meantime, since the BRDF varies versus lighting angle, viewing angle and wavelength, the measured data is very huge and inconvenient to store and use, therefore, it is very urgent to build a precise parameter model of the BRDF based on the measured data [16,17]. In order to extend the measuring angle range further and use the measured BRDF data expediently, it is very important to make researches on measurement and modeling of bidirectional reflectance distribution function.

* Corresponding author. Address: 2 Yikuang Street, Nan Gang District, Harbin 150080, China. Tel.: +86 451 86414883 728(O), mobile: +86 18645003725; fax: +86 451 86416315.
*E-mail addresses:* fountainhy@hit.edu.cn, fountainhy@163.com (H. Wang).

0263-2241/$ - see front matter © 2013 Elsevier Ltd. All rights reserved.
http://dx.doi.org/10.1016/j.measurement.2013.07.008

## 2. Measurement of BRDF

### 2.1. Definition of BRDF

The bidirectional reflectance distribution function $f_r(\theta_i, \varphi_i; \theta_r, \varphi_r, \lambda)$ is an expression of the physical property of a material, which describes the pattern of light reflected from a surface of the material to all directions above the surface, for all directions of incident light. It is a five-dimensional function about incident zenith angle $\theta_i$, reflected zenith angle $\theta_r$, incident azimuth angle $\varphi_i$, reflected azimuth angle $\varphi_r$ and wavelength $\lambda$. For a material surface and a certain wavelength, the BRDF determines the appearance of materials for different viewing directions, which is defined as the ratio of the radiance $dL_r(\theta_r, \varphi_r)$ reflected from a surface in the direction $(\theta_r, \varphi_r)$ to the incident irradiance $dE_i(\theta_i, \varphi_i)$ onto the surface from the direction $(\theta_i, \varphi_i)$ (see Fig. 1) [18].

$$f_r(\theta_i, \varphi_i; \theta_r, \varphi_r) = \frac{dL_r(\theta_r, \varphi_r)}{dE_i(\theta_i, \varphi_i)} \tag{1}$$

where radiance $dL_r(\theta_r, \varphi_r)$ is the radiant power flow per unit solid angle and unit area normal to the reflected rays and has the unit (W/m$^2$ sr), and irradiance $dE_i(\theta_i, \varphi_i)$ is the power flux density irradiating a surface per unit area and has unit (W/m$^2$).

### 2.2. Measuring method

#### 2.2.1. Measuring principle

According to BRDF definition, absolute measurement of BRDF is to measure incident spectral irradiance and reflected spectral radiance by illuminance meter and luminance meter respectively.

The incoming irradiance $E_e$ on the sample surface can be achieved in terms of incident power of light source $P_i$ and illuminated area $A$ of the sample. The received radiance $L_e$ on the detector can be calculated using received power $P_s$, detecting solid angle $\Omega$ and received area $A\cos\theta_s$. Then the BRDF of test sample surface can be obtained according to the ratio of $L_e$ and $E_e$, namely [14,19],

$$\mathrm{BRDF} = \frac{L_e}{E_e} = \frac{(P_s/\Omega A\cos\theta_s)}{(P_i/A)} = \frac{P_s}{P_i\Omega\cos\theta_s}(\mathrm{sr}^{-1}) \tag{2}$$

#### 2.2.2. Measuring scheme

The schematic design of BRDF absolute measurement is shown in Fig. 2. The lighting source is fixed on the support arm which is set in the cantilever with a slide rail, and the test sample is put on the sample stage. The detector is placed on the measurement platform. The different lighting angle and viewing angle can be obtained by pitching and horizontal rotating of the sample stage and horizontal rotating of the cantilever. The whole measuring process is completed automatically under computer control to enhance the measuring accuracy and sampling speed.

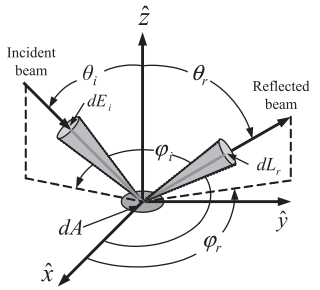


**Fig. 1.** Light reflection geometry.

#### 2.2.3. Measuring equipment

The measuring device consists of illuminating system, detection system, mechanical system and control system according to the measuring scheme of BRDF [15,20]. The whole measuring equipment is described in Fig. 3.

### 2.3. Measuring results

As an example, when incident zenith angle is 30°, 45° and 60°, reflected zenith angle is 0–85° and wavelength is 380–760 nm, the absolute measuring experiments of BRDF on yellow tinfoil, black ceramic tile are made respectively. The relationship of BRDF, wavelength and reflected zenith angle are obtained. The experimental results show that the test materials present apparent specular reflection characteristics. The BRDF increases with an increase of incident zenith angle, and the reflected beam becomes narrow, which indicates the reflected energy is more concentrated, as are shown in Figs. 4 and 5.

### 2.4. Measuring error

There are several factors influencing the error of the BRDF measurement. The error $\varepsilon_{\mathrm{BRDF}}$ can be expressed:

$$\varepsilon^2_{\mathrm{BRDF}} = \varepsilon^2_{ME} + \varepsilon^2_{IE} + \varepsilon^2_{DE} + \varepsilon^2_{PE} \tag{3}$$

where $\varepsilon_{ME}$ is the mechanical system error; $\varepsilon_{IE}$ is the illuminating system error; $\varepsilon_{DE}$ is the detection system error and $\varepsilon_{PE}$ is the personal error.

The mechanical system error $\varepsilon_{ME}$ is:

$$\varepsilon^2_{ME} = \varepsilon^2_{re} + \varepsilon^2_{he} + \varepsilon^2_{de} \tag{4}$$

Where $\varepsilon_{re}$ is the rotation error of the motorized precision rotary stages and it is less than 0.0003° for MRS101 and 0.0002° for MRS103; $\varepsilon_{he}$ is the height error of the holder and it is 0.03 mm; $\varepsilon_{de}$ is the displacement error of the detector and it is 0.01 mm. According to the definition of error, the mechanical system error $\varepsilon_{ME}$ is less than 3.34%.

The illuminating system error $\varepsilon_{IE}$ is:

$$\varepsilon^2_{IE} = \varepsilon^2_{il} + \varepsilon^2_{rl} + \varepsilon^2_{sl} \tag{5}$$

where $\varepsilon_{il}$ is the error from the stability of the illuminating light source and it is 0.1%; $\varepsilon_{rl}$ is the error from the time-variation of the reflected luminance and it is 0.4%; $\varepsilon_{sl}$ is the error from stray light and it is controlled within 1% during the experimental process. Taking all the above factors into account, the illuminating system error $\varepsilon_{IE}$ is less than 1.08%.

The detection system error $\varepsilon_{DE}$ is:

$$\varepsilon^2_{DE} = \varepsilon^2_{snr} + \varepsilon^2_{nl} + \varepsilon^2_{sld} \tag{6}$$

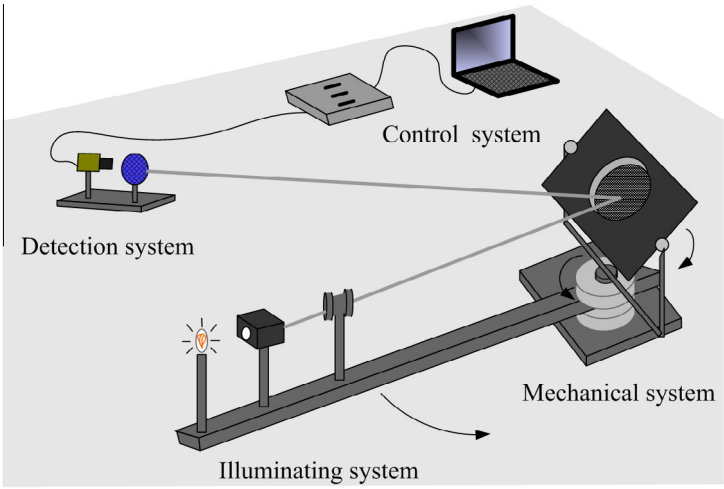


**Fig. 2.** Schematic design of BRDF absolute measurement.

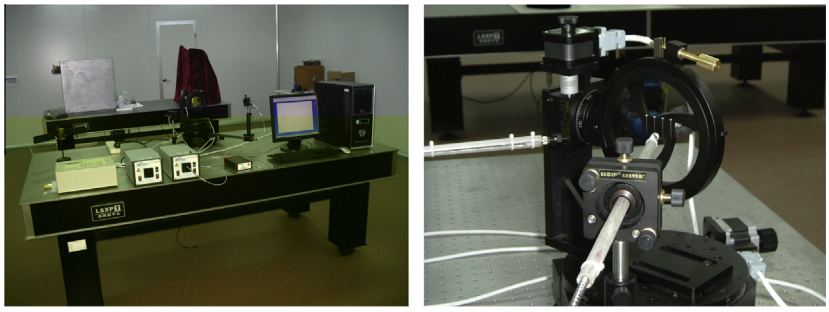

**Fig. 3.** Measuring equipment of the BRDF.

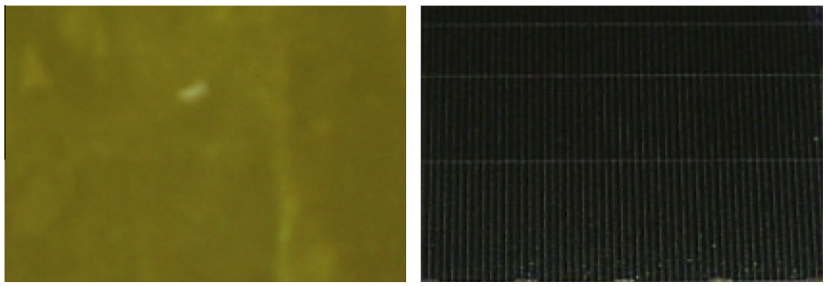


**Fig. 4.** Test materials.

where $\varepsilon_{snr}$ is the error due to the signal to noise ratio and it is 0.004 for both incident power measurement and reflected power measurement; $\varepsilon_{nl}$ is the non-linear error of the detector and it is about 0.4%; $\varepsilon_{sld}$ is the receiver solid angle error and the error stems from the $z$-direction misalignment and the receiver's aperture. The actual measurement shows the $z$-direction misalignment error is 0.2 mm and the aperture is 0.15%, then the receiver solid angle error is 0.7%. So the detection system error is less than 0.9%.

The personal error $\varepsilon_{PE}$ is caused by different readers, according to the actual measurement of several samples, it is 4.84%.

Based on above experimental conditions, the overall error in the experiment is:

$$\varepsilon_{\mathrm{BRDF}} = \sqrt{\varepsilon_{ME}^2 + \varepsilon_{IE}^2 + \varepsilon_{DE}^2 + \varepsilon_{PE}^2} \approx 6.05\% \tag{7}$$

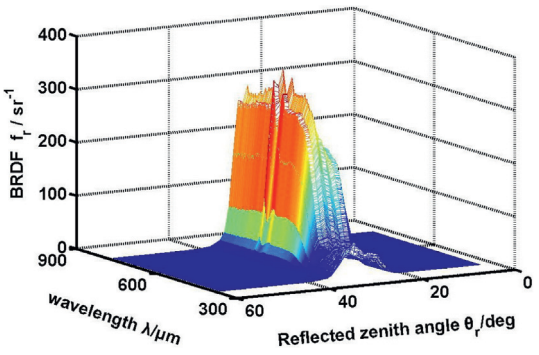


(a) Incident angle 30°, yellow tinfoil

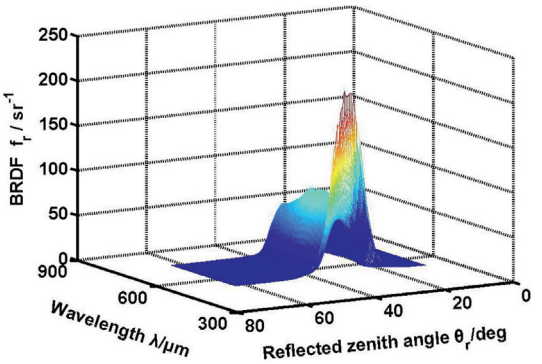


(b) Incident angle 30°, black ceramic tile

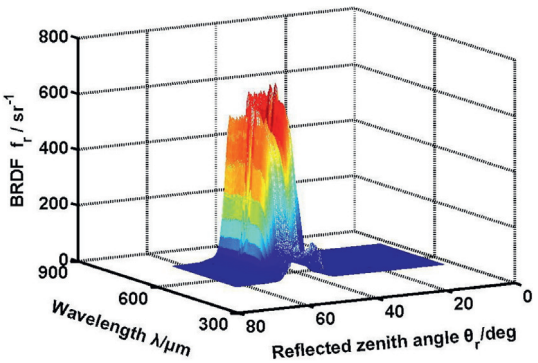


(c) Incident angle 45°, yellow tinfoil

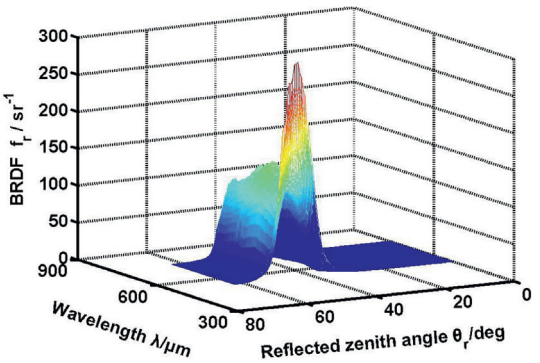


(d) Incident angle 45°, black ceramic tile

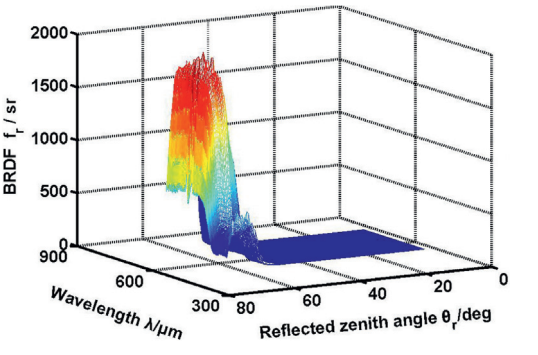


(e) Incident angle 60°, yellow tinfoil

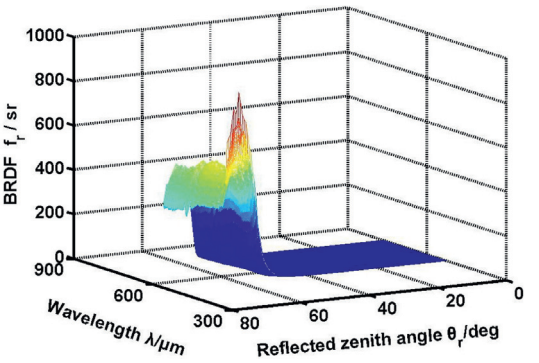


(f) Incident angle 60°, black ceramic tile

**Fig. 5.** Relationship of BRDF, wavelength and reflected angle for test materials.

## 3. Modeling of BRDF

### 3.1. Parameter model

According to surface characteristics of the material, any local illumination area $\Delta A$ of the material surface can be divided into a great many microfacets and each microfacet is so sufficiently smooth that it can be replaced with its local tangent plane. In addition, the size of each microfacet is much larger than the visible wavelength, so the light diffraction can be ignored. The normal direction of each microfacet $\hat{n}$ is in the upper hemispherical space, as is shown in Fig. 6. Based on geometrical optics principle, the BRDF of the material surface can be regarded as a constitution of specular reflection and diffuse reflection of the tangent planes, and that the diffuse reflection component follows Lambert's law. The concrete expression is as follows [21]:

$$f_r = k_s \frac{DGF(\theta_i, \lambda)}{\pi \cos\theta_i \cos\theta_r} + \frac{k_d}{\pi} \tag{8}$$

where $D$ is the distribution function of the microfacets; $G$ is the geometrical attenuation factor; $F(\theta_i, \lambda)$ is the Fresnel

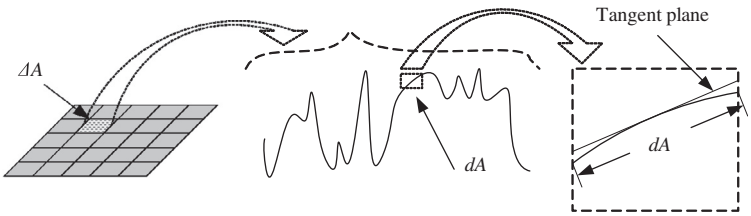


**Fig. 6.** Microstructure analysis of the material surface.

reflection coefficient; $k_s$ is the specular reflection coefficient; $k_d$ is the diffuse reflection coefficient.

The first part and the second part represent the specular reflection and diffuse reflection components of the local illumination area respectively in formula (8). It is able to model the reflection from a wide variety of surfaces and is computationally convenient.

*3.1.1. Distribution function of the microfacets*

The distribution function of the microfacets describes the smooth level of the material surface and is called roughness factor. In order to describe the surface appearance of the material, the distribution function of the microfacets based on Torrance–Sparrow five-parameter model and Beckmann slope distribution function is built according to the attribute of the test material (see Fig. 7). $\hat{s}$ is the incident vector, $\hat{v}$ is reflected vector and $\hat{n}$ is the normal vector of the local illumination area. $\hat{a}$ is the unit vector bisecting incident and reflected direction, namely, it denotes the normal direction of the microfacet. The expression of the distribution function of the microfacets is:

$$D = \exp[c(1-\cos\gamma)^d] \tag{9}$$

where $c$ and $d$ is the undetermined parameters, $\gamma$ is the included angle of incident light and normal of the microfacet. $\gamma$ can be expressed as follows:

$$\cos\gamma = \sqrt{(\cos\theta_i\cos\theta_r - \sin\theta_i\sin\theta_r\cos\varphi + 1)/2} \tag{10}$$

where $\varphi$ is the included angle of incident and reflected azimuth angle, $\varphi = \varphi_r - \varphi_i$.

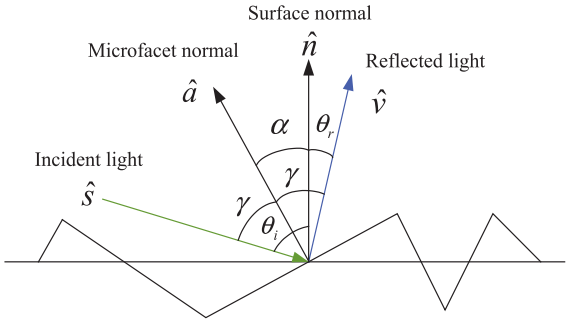


**Fig. 7.** Distribution of the microfacets.

*3.1.2. Geometrical attenuation factor*

Shadowing and masking phenomenon will occur among the adjacent microfacets when the incident angle or observed angle is large and the reflected flux of the microfacets will change. Shadowing denotes that the light incident on the microfacet is cut off and masking denotes that the light reflected by the microfacet is cut off in the observed direction (see Fig. 8). The geometrical attenuation factor is introduced in the reflected energy calculation to describe the shadowing and masking effect. The mathematical expression is:

$$G = \sqrt{\tan^2\theta_i + \tan^2\theta_r - 2\tan\theta_i\tan\theta_r\cos\varphi} \tag{11}$$

*3.1.3. Fresnel reflection coefficient*

The Fresnel reflection coefficient is usually obtained by Fresnel formula, but the refractive index for corresponding wavelength must be measured in advance. For convenience, the power exponent function formula that can simulate measured data precisely in the entire incident angle range is introduced to substitute for Fresnel formula. The concrete expression of the power exponent function formula is:

$$F(\theta_i,\lambda) = \exp[a(b-\cos\theta_i)^2] \tag{12}$$

where $a$ and $b$ are the undetermined parameters.

*3.2. Data fitting*

*3.2.1. Optimization algorithm*

Simulated annealing algorithm (SAA) is adopted to achieve the model parameters. SAA is a random search algorithm based on the Monte Carlo iterative computation method and the globally optimal solution can be found during the simulated annealing process. So-called optimization is the procedure to find the minimal or maximal solution of the object function in solution space. The optimization criterion of model parameter selection in this pa-

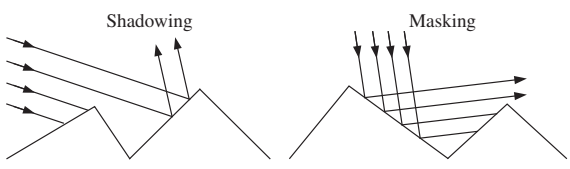


**Fig. 8.** Shadowing and masking of the microfacets.

per is that the standard mean-square error of simulated measured data is the least. The least mean-square error is denoted as follows, namely the object function [22].

$$E(x) = \frac{\sum_{\theta_i}\sum_{\theta_r} g_1(\theta_i) g_2(\theta_r)[f_{r\text{-model}}(\theta_i,\theta_r,\varphi_r) - f_{r\text{-measured}}(\theta_i,\theta_r,\varphi_r)]^2}{\sum_{\theta_i}\sum_{\theta_r} g_1(\theta_i) g_2(\theta_r)[f_{r\text{-measured}}(\theta_i,\theta_r,\varphi_r)]^2} \tag{13}$$

where $x = [a, b, c, d, k_s, k_d]^T$ is the column vector; $f_{r\text{-measured}}$ is the measured BRDF data; $f_{r\text{-model}}$ is the calculated BRDF data; $g_1(\theta_i)$ and $g_2(\theta_r)$ is weight function.

More precisely empirical parameters can be obtained for inhomogeneous measuring interval in important incident and observed region by selecting weight function in some way and adjusting influence of each error on total error. Experimental data is measured in equal interval in this paper and the weight function selected is usually equal to 1.

**Table 1**
BRDF model parameters of the surface material.

| Material type | $a$ | $b$ | $c$ | $d$ | $k_s$ | $k_d$ |
|---|---|---|---|---|---|---|
| Yellow tin foil | 3.87 | 0.5216 | −300 | 0.74 | 451.7958 | 1.3034 |
| Black ceramic tile | 7.9678 | 0.5555 | −180 | 0.74 | 190.5 | 1.8667 |

*3.2.2. Optimization results*

Supposing that the object function is less than 0.01, according to the measured data of BRDF, BRDF model parameters of the surface material are achieved based on simulated annealing algorithm, the results are shown in Table 1.

*3.3. Fitting error*

*3.3.1. Comparison of modeling and measured results*

The Comparison of BRDF modeling and measured results is shown in Figs. 9–11. The figures indicate that the BRDF model results fit well with the BRDF measured results.

*3.3.2. Fitting error*

Relative root-mean-square error is selected to analyze fitting error [12].

$$\sigma_r = \sqrt{\frac{1}{N}\sum\left(\frac{f_{r\text{-model}} - f_{r\text{-measured}}}{f_{r\text{-measured}}}\right)^2} \tag{14}$$

*3.3.3. Error results*

According to the theoretical calculation results of the BRDF model and the measured data of the BRDF experiment, fitting error of the model at the angle 30°, 45°, 60°

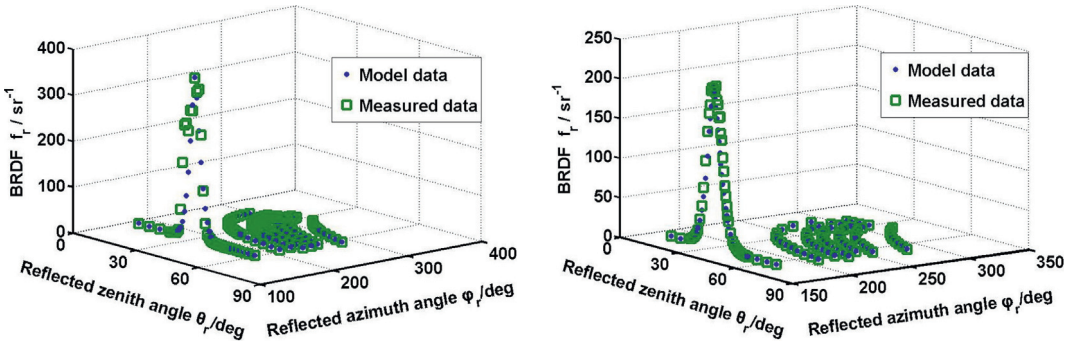


(a) Yellow tin foil (b) Black ceramic tile

**Fig. 9.** Comparison between measured data and model data of BRDF at angle30°.

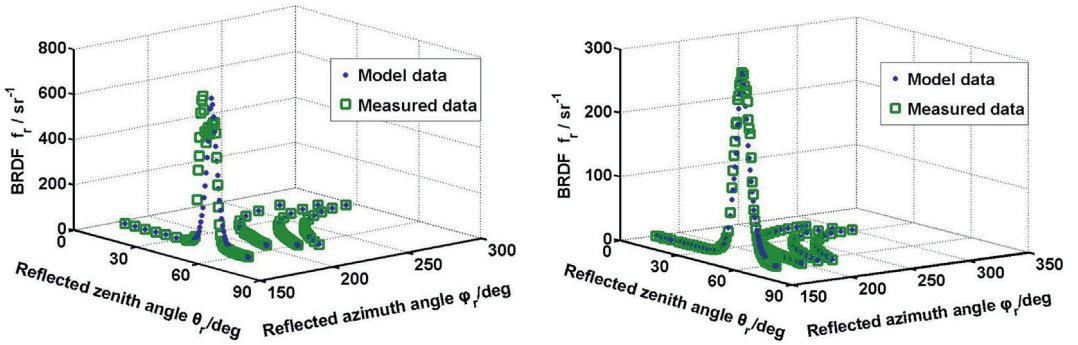


(a) Yellow tin foil (b) Black ceramic tile

**Fig. 10.** Comparison between measured data and model data of BRDF at angle 45°.

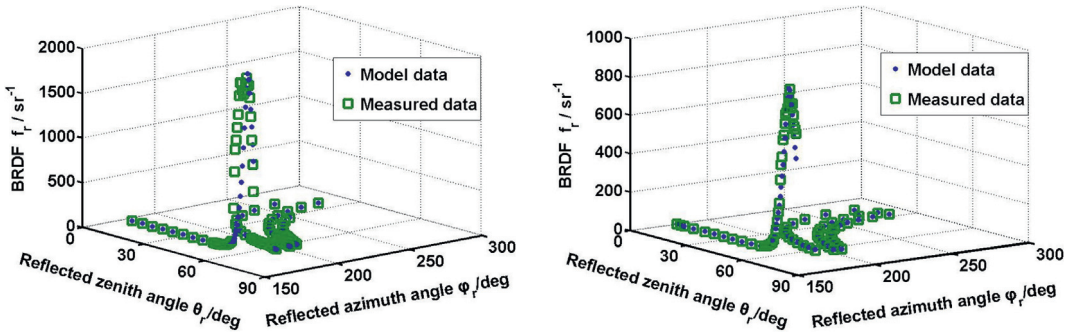


(a) Yellow tin foil (b) Black ceramic tile

**Fig. 11.** Comparison between measured data and model data of BRDF at angle 60°.

**Table 2**
Results of fitting error.

| Material type | Incident light $\theta_i$ (°) | Relative RMS error $\sigma_r$ (%) |
|---|---|---|
| Yellow tin foil | 30 | 8.82 |
| | 45 | 9.94 |
| | 60 | 9.53 |
| Black ceramic tile | 30 | 8.84 |
| | 45 | 8.75 |
| | 60 | 8.41 |

can be calculated by the above fitting error analysis method, as are shown in Table 2.

## 4. Conclusions

According to BRDF definition, a measurement platform of BRDF is set up based on the AvaSpec-2048 microscopic fiber spectrometer. The measurement software and control software is integrated by developing an interface software, which realizes the automatic measurement of BRDF. The spectral measurement range of the device is 200–1100 nm and the spectral resolution is 2.4 nm. The angular measurement range is 0–85° in zenith angle and 0–360° in azimuth angle and the angle resolution is 0.01°. The parameter model of BRDF is built through fitting processing of measured data based on the simulated annealing algorithm. Fitting error analysis of the BRDF parameter model is done and the maximal fitting error is 9.94%. The modeling of BRDF solves the problem that measured data of BRDF is great large and actual application of BRDF is inconvenient. On the whole, the study on measurement and modeling of BRDF provides an effective supplementary means to real-time image generation of computer graphics and real-time energy calculation of target characteristics. However, there must be a more or less angle limitation only depending on the measurement experiment even if the measuring equipment is improved, so it is quite valuable to find a more precise method to extend measured data.

## Acknowledgement

This work was supported by the National High Technology Research and Development Program of China (Grant No. 2006AA704214).

## References

[1] J.D. Lawrence, Acquisition and Representation of Material Appearance for Editing and Rendering, PhD Dissertation, Princeton University, 2006, pp. 20–36.
[2] J. Kainulainen, Reflection Models in Real-Time Graphics, Master Thesis, Helsinki University, 2003, pp. 15–48.
[3] G.T. Georgiev, C.K. Gatebe, J.J. Butler, M.D. King, Comparison between laboratory and airborne BRDF measurements for remote sensing, Proc. SPIE 6296 (2006) 301–310.
[4] Y. Boucher, Comparison of measured and modeled BRDF of natural targets, Proc. SPIE 3699 (1999).
[5] Z. Otremba, J. Piskozub, Modeling the bidirectional reflectance distribution function (BRDF) of seawater polluted by an oil film, Opt. Exp. 12 (2004) 1671–1676.
[6] B.W. Kimmel, G.V.G. Baranoski, A novel approach for simulating light interaction with particulate materials: application to the modeling of sand spectral properties, Opt. Exp. 15 (2007) 9755–9777.
[7] T.A. Germer, M.E. Nadal, Modeling the appearance of special effect pigment coatings, in: Z.-H. Gu, A.A. Maradudin (Eds.), Surface Scattering and Diffraction for Advanced Metrology, Proc. SPIE 4447 (2001) 77–86.
[8] P. Boher, T. Leroux, T. Bignon. Spectral BRDF of color shifting paints and e-papers using multispectral Fourier optics instrument, in: SID Conference Record of the International Display Research Conference, 2011, pp. 116–119.
[9] L. Bai, Z.S. Wu, X.R. Zou, Y.H. Cao, Seven-parameter statistical model for BRDF in the UV band, Opt. Exp. 20 (11) (2012) 12085–12094.
[10] R. Lu, J.J. Koenderink, A.M.L. Kappers, Optical properties (bidirectional reflectance distribution function) of shot fabric, Appl. Opt. 39 (2000) 5785–5795.
[11] A. Bhandari, B. Hamre, O. Frette, L. Zhao, J.J. Stamnes, M. Kildemo, Bidirectional reflectance distribution function of Spectralon white reflectance standard illuminated by incoherent unpolarized and plane-polarized light, Appl. Opt. 50 (2011) 2431–2442.
[12] J.E. Hubbs, L.D. Brooks, M.J. Nofziger, F.O. Bartell, W.L. Wolfe, Bidirectional reflectance distribution function of the Infrared Astronomical Satellite solar-shield material, Appl. Opt. 21 (1982) 3323–3325.
[13] M.A. Cauquya, M.C. Roggemanna, T.J. Schulz, Approaches for processing spectral measurements of reflected sunlight for space situational awareness, Proc. SPIE 5428 (2004) 48–57.
[14] G.T. Georgiev, J.J. Butler, Laboratory-based bidirectional reflectance distribution functions of radiometric tarps, Appl. Opt. 47 (2008) 3313–3323.
[15] K.J. Voss, A. Chapin, M. Monti, H. Zhang, Instrument to measure the bidirectional reflectance distribution function of surfaces, Appl. Opt. 39 (2000) 6197–6206.
[16] L. Simonot, G. Obein, Geometrical considerations in analyzing isotropic or anisotropic surface reflections, Appl. Opt. 46 (2007) 2615–2623.
[17] G.E. Renhorn, G.D. Boreman, Analytical fitting model for rough-surface BRDF, Opt. Exp. 16 (2008) 12892–12898.
[18] F.E. Nicodemus, J.C. Richmond, J.J. Hsia, I W. Ginsburg, T. Limperis, Geometrical considerations and nomenclature for reflectance, in:

National Bureau of Standards, NBS monograph, vol. 160, October 1977.
[19] J.C. Stover, Optical scattering: measurement and analysis, SPIE 5 (1995) 1–5.
[20] L. Ke, A Method of Light Reflectance Measurement, Master's Thesis, University of British Columbia, 1999, pp. 16–21.
[21] R.C. Love, Surface Reflection Model Estimation from Naturally Illuminated Image Sequences, PhD Dissertation, University of Leeds, 1997, pp. 22–39.
[22] S. Kirkpatrick, C.D. Gelatt, M.P. Vecchi, Optimization by simulated annealing, Science, New Ser. 220 (1983) 671–680.